Influences of Complex Topography and Biochemistry on Mesenchymal Stem Cell Differentiation

Yang, Liangliang

DOI:
10.33612/diss.146104615

CHAPTER 4

Decoupling Amplitude and Wavelength of Anisotropic Topography and the Influence on Osteogenic Differentiation of Mesenchymal Stem Cells Using a High-throughput Screening Approach

This chapter has been published in:

Liangliang Yang, Lu Ge, Qihui Zhou, Klaudia Malgorzata Jurczak, Patrick van Rijn*. *ACS Appl. Bio Mater.* **2020**, 3, 3690−3697.

Abstract

High-throughput screening (HTS) methods based on anisotropically topography gradients have been broadly used to investigate the interactions between cells and biomaterials. However, few studies focus on the optimum parameters of topography for osteogenic differentiation since the structures of topography are complex with multiple combinations of parameters. In this study, we developed polydimethylsiloxane (PDMS)-based wrinkled topography gradients (amplitudes between 144 and 2854 nm and wavelengths between 0.91 and 13.62 μm), and decoupled the wavelength and amplitude via imprinting lithography and shielded plasma oxidation. The PDMS wrinkle gradient was then integrated with the bottomless 96-well plate to constitute the wrinkled HTS platform, which consists of 70 different wrinkle parameters. From the *in vitro* culture of bone marrow stem cells, it was observed that aligned topography has an important influence on the macroscopic cell behavior (i.e., cell area, elongation, and nucleus area). Furthermore, the optimum wrinkle parameter (wavelength: 1.91 μm; amplitude: 360 nm) for osteogenic differentiation of stem cells was determined via this screening plate approach. This screening platform is not only beneficial for a better understanding of the interactions between topography and biomaterials, but also advances the development of bone tissue engineering developments.

Keywords: high-throughput screening, topographical gradient, stem cell, osteogenic differentiation, materiobiology

4.1 Introduction

The key for the development of biomaterials in tissue engineering and regenerative medicine is the ability to use the physicochemical properties to control cell behavior[1]. Mesenchymal stem cells (MSCs) are an interesting cell type because of their autologous availability[2], capacity to differentiate into multilineage potential (adipogenic, osteogenic, and chondrogenic differentiation)[2] and low immunogenic reaction by allogeneic hosts[3]. Therefore, controlling the differentiation behavior of MSCs is vital in many biological aspects such as bone regeneration[4]. MSCs could perceive the physical or topographical signals from the extracellular matrix (ECM), and respond to these signals and thereby influencing cell responses, including adhesion, proliferation, migration, and differentiation[5–11]. The surface topography significantly affects cell behavior through contact guidance[12], and the cell is able to sense such surface parameters between 10 nm and 100 μm[13,14]. Previous studies demonstrate that enhanced osteogenic differentiation stimulated by topography is caused by the more formation of focal adhesion, activation of RhoA/Rock signaling pathway[15,16], and the regulation of microRNA[5]. Furthermore, researchers also revealed that topography-induced integrin-linked kinase (ILK)/β-catenin pathway[17], ILK/ extracellular signal-regulated kinase 1/2 and ILK/p38[18], and crosstalk between focal adhesion kinase/mitogen-activated protein kinase and ILK/β-Catenin pathways[19] facilitate osteogenesis of stem cells.

In vivo, the ECM of most tissues, for instance, bone, tendon, and nerve, have anisotropic architectures composed of aligned nano/micro-scaled structures[20–23]. There are various studies focused on the impact of anisotropic structures on the differentiation of stem cells. Kukumberg et al.[24] investigated the influence of anisotropic topography on the endothelial differentiation of MSCs, and found that the 1.8 μm diameter convex microlens pattern combined with the vascular endothelial growth factor (VEGF) was found to be most efficient for differentiation. Tan and co-workers[25] prepared a multi-architecture chip with different topographical structures and parameters to study the neuron differentiation of neural progenitor cells. The data revealed that the different combinations of parameters (grating, spacing, height) triggered cells towards varied degree of neuronal differentiation. These studies illustrate that topography with specific parameters enhances osteogenic and neuronal differentiation. However, it should be noted that many of these studies use topographies with parameters that are relatively chosen arbitrarily, which provided significant yet limited information. Furthermore, the structures mentioned above are extremely complex with various combinations of topography parameters (i.e., groove, ridge, and pitch); therefore, the parameters that play an important role in guiding cell behavior are not exactly known unless these parameters are decoupled. Therefore, in order to better understand the relevant topographical features, it is essential to systematically change one parameter to determine its influence on cellular behaviors.

Surface topographical gradients provide an ideal platform to study cell behavior in a HTS manner. This method is time and cost-efficient, and minimizes systematic or methodological errors[26]. Furthermore, the platform can screen for the optimum topographical parameters for promoting specific cellular processes[26–29]. Previously, our group studied cell contact guidance using micro/nano-topographical gradients and found that the parameter of topography has an essential effect on various cell activity, for example, cell orientation, elongation, migration and differentiation[30–37]. The wavy-like wrinkle structure is a powerful tool for engineering nano- and microstructures in a cost-effective way[38,39]. In addition, the grating structure consists of sharp corners or edges that may not be supportive for cells[38,39]. Furthermore, wrinkles consists of two parameters namely wavelength and amplitude, and these two parameters have always been coupled in previous studies. However, by decoupling the wavelength and amplitude, specific insights in individual contributions of topography parameters may be gained.

In this study, we hypothesize that both wavelength and pitch contribute to topography-mediated cell stimulation. To investigate these individual contributions of topography parameters, we prepared a HTS platform consisting of 70 different combinations of wavelengths and amplitudes in one 96-well plate, following work by van der Boon et al..[40] By sequentially preparing aligned topography gradients via a silicone stretch-oxidation-release method and imprinting lithography, followed by selective amplitude reduction using plasma oxidation for different durations, amplitude and wavelength were decoupled and the whole substrate was integrated into standardized well-plate technology. Using the multi-parameter topography well plate, the optimum wavelength/amplitude combination for osteogenesis of human bone marrow-derived mesenchymal stem cells (hBM-MSCs) was investigated. The wrinkle parameters were characterized by atomic force microscopy (AFM). hBM-MSCs were seeded to study the influences of wrinkle parameters on macroscopic cell behavior (i.e., cell area, cell elongation, and nucleus area), and osteogenic differentiation, which was examined by immunofluorescent staining of alkaline phosphate (ALP) and Alizarin Red staining,

respectively. This HTS platform facilitates the understanding of the relationships between bio-interface and biological behavior, and the screening capability provides great potential for the designing of biomaterials.

4.2 Methods

4.2.1 PDMS film preparation and wrinkle gradient formation

PDMS film and wrinkle gradient were prepared as described previously[30,41]. Briefly, PDMS substrate was fabricated by mixing the liquid PDMS precursor and curing agent (Sylgard 184, Dow Corning) by weight ratio of 10:1. The mixtures were degassed for 15 min to remove air bubbles, and cured at 70 °C overnight. For the wrinkled gradient, the cured PDMS (10.5 × 9 cm) was stretched uniaxially to 120% of the original length, then the surface was covered with a right angled triangular prism mask (10 × 8 cm, with an angular aperture of 30°) and oxidized in air plasma (Plasma Activate Flecto 10 USB, maximum intensity) for 650 s at 25 mTorr. After oxidation, a glassy layer (SiO_2) is formed on the surface of substrate, and due to the shielded role of the mask the thickness of the SiO_2 layer decreases from the most exposed side (mask opening) to the least exposed side. The mask dimensions provide control over the oxidation gradient development. Afterwards, the strain was released, inducing the formation of wrinkled gradient, and the wrinkle wavelength and amplitude increased from the lowest oxidized region (closed side) to the highest oxidized region (open side of the mask). All substrates were further oxidized for 10 min under the pressure 100−150 mTorr to make the surface completely oxidized, which was beneficial for the imprinting process.

4.2.2 Imprinting

The fabricated PDMS wrinkle gradient was used as mold, and a fresh mixture of precursor and curing agent (weight ratio of 10:1) was poured onto it, followed by overnight curing at 70 °C. Afterwards, the mold was removed and the newly prepared substrate with wrinkle gradient was used for further study.

4.2.3 Decouple the wavelength and amplitude

After imprinting, the fresh PDMS membrane has again the elastomeric properties rather than the oxidized surface of the mold while the same wrinkle structures as the mold are still present. Then the soft PDMS membrane was oxidized with a flat mask for different time (0 s, 5 s, 10 s, 20 s, 1 min, 2 min and 10 min). Longer plasma oxidation time resulted in more reduction in amplitude of the wrinkles. After that, the PDMS substrate was imprinted again to ensure the surface chemical and mechanical properties are the same for all samples. The substrates were further oxidized by plasma at 500 mTorr for 1 min and used for integrating it into the well plate. The flat substrate (10:1 for the ratio of precursor and curing agent) was prepared and oxidized with same condition of plasma mentioned above, to confirm all the substrates have the same chemical and mechanical properties.

4.2.4 PDMS surface characterization

Topography images were obtained by atomic force microscope (AFM, Nanoscope V Dimension 3100 microscope, Veeco, United States) performed with tapping mode in the air (DNP-10 tip). The wavelength and amplitude of the wrinkle gradient were determined by NanoScope Analysis software.

4.2.5 Well plate embedding

The bottomless 96-well plate embedded with PDMS membrane was prepared as described previously[40]. Briefly, the samples for wrinkle gradient were cut into size of 9.6 × 7.5 cm, to cover wells A1−H1 through columns 1−10 of the plate (Greiner Bio-One no. 655101), and column 11 was sacrificed to connect the wrinkle gradient with column 12, which acts as flat control (1.5 × 7.5 cm) (**Figure S1**). Then the area of the plate bottom was coated with liquid mixture of precursor and curing agent, and the plate was put into the oven for the mixture to form a glue-like state. The two substrates were carefully placed on the top of the glue, and pressed firmly to make sure a good connection is produced. At last, ~32 g of PDMS mixture was poured on the top of the bottom . Samples were cured at 70 °C for 3 hours to seal the bottom.

4.2.6 Cell culture

hBM-MSCs obtained from Lonza were used for the experiments. hBM-MSCs were cultured in proliferation medium comprising Alpha modified Eagle medium (Gibco), 10% fetal bovine serum (Gibco), 0.1% ascorbic acid 2-phosphate (Sigma) and 1% penicillin/streptomycin (Gibco). Cells were cultured at 37 °C in the presence of 5% CO_2. The medium was refreshed every three days and cells were detached with trypsin and

harvested at 80% confluence. hBM-MSCs of passage 4 were used for all of the experiments.

4.2.7 Immunostaining

The embedded well plate was sterilized by 75% ethanol and then washed with Dulbecco's phosphate-buffered saline (DPBS). Afterwards, 2500 cells of hBM-MSCs were seeded in each well. For immunostaining, hBM-MSCs seeded on the different topographical patterns were fixed in 3.7% paraformaldehyde (PFA, Sigma) solution for 20 min at room temperature, and subsequently permeabilized with 0.5% Triton X-100 (Sigma) solution for 3 min and incubated with 5% bovine serum albumin (BSA, Sigma) in PBS for 30 min. Then, the cells were stained with primary anti-ALP antibody (Developmental Hybridoma Bank, B4-78, 1:100) for 1 h, and secondary Rhodamine Red™-X-conjugated goat-anti-mouse antibody (Jackson Immunolab, 1:100) and 4' 6 - diamidino - 2 - phenylindole (DAPI), TRITC-phalloidin for 1 hour. Finally, the images were taken with TissueFaxs (Tissue-Gnostics GmbH, Vienna, Austria). Cell area and nucleus area was determined by TissueQuest. Cell elongation was calculated as the ratio between the length of the cell major axis and length of the minor axis (for the quantification of cell area, nucleus area, and cell elongation, ≥ 60 cells for each sample and 3 independent experiment were analyzed).

4.2.8 Osteogenic differentiation of MSCs

hBM-MSCs were seeded onto substrates at a cell density of 2500 cells/well. All plates were stored in an incubator at 37 °C, 5% CO_2, and after 24 h the medium was exchanged for osteogenic differentiation medium (OM) composed of growth medium and osteogenic supplements (10 mM glycerophosphate (Sigma) and 100 nM dexamethasone (Sigma)) for 14–21 days. The culture medium was replaced every 3 days. ALP and nucleus staining were performed by the method of mentioned above.

To further examine osteogenesis, mineralization of the ECM was stained by Alizarin Red after 21 days under OM. The samples were washed twice with DPBS, fixed with 4% PFA for 15 minutes and then 0.1% Alizarin Red solution was added into the wells. After 30 min, the wells were washed with DPBS to remove the excess of Alizarin Red solution. For a quantitative analysis, the cultures stained with Alizarin Red were de-stained with 10% cetylpyridinum chloride in 10 mM sodium phosphate buffer for 30 minutes to release the bound calcium. The supernatant was collected and a microplate reader (BMG LABTECH, Offenburg, Germany) was used to measure the absorbance at 540 nm. The values were normalized for the cell numbers for each well, and cell number was quantified by nucleus stained with DAPI through TissueQuest.

4.2.9 Statistics

All values are expressed as the mean ± standard deviation. Origin 9.0 software was used to perform statistical analysis. One-way analysis of variance (ANOVA) was used with Tukey's test to identify differences between groups. *$P < 0.05$, **$P < 0.01$, and ***$P < 0.001$, respectively.

4.3 Results and Discussion

4.3.1 Preparation of wrinkle gradient and surface characterization

The preparation process for the topographical gradient is illustrated in **Figure 1**. During the process, PDMS substrate was uniaxially stretched and plasma oxidized with the surface being shielded using a right-angled triangular prism mask. After releasing the strain, the wrinkle gradient forms, and the wrinkle parameters were tunable by changing the oxidation time, angle of the mask as well as pressure. The wrinkle size increased with increasing plasma exposure occurring from the least exposed side to the most exposed side, and the largest wrinkle dimensions were observed when extending to the area without mask (fully exposed to plasma). It has to be noted that the amplitude and wavelength are always coupled, and larger wavelengths are correlated with higher amplitudes.

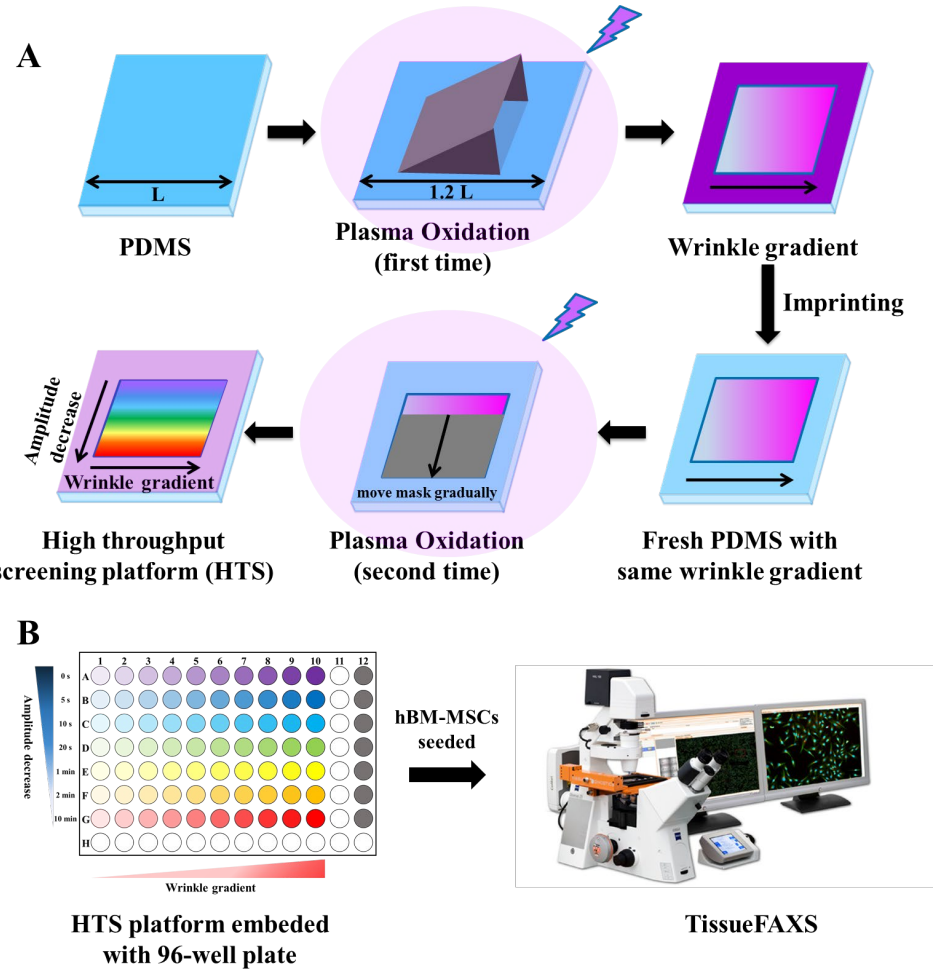

Figure 1. (A) Schematic diagrams of the formation of high throughput screening platform by air plasma oxidation. The PDMS membrane was stretched uniaxially to 120% of the original length, followed by covering with a mask and oxidized in air plasma (first time). After oxidation, releasing the strain induced the formation of wrinkled gradient. After imprinting, the new soft PDMS membrane was oxidized to decrease the amplitude or decouple the wavelength and amplitude. (B) The HTS platform was integrated with bottomless 96-well plate and suitable for using in commercially available imaging systems such as the TissueFax..

The surface features after imprinting (before the second oxidation treatment) were characterized by AFM, as shown in **Figure 2A**. The anisotropic gradients were prepared with amplitudes ranging from 144 to 2854 nm and wavelengths between 0.91 and 13.62 μm, as shown in **Figures 2B** and **2C** where the numbers depict the column number of the final position in the 96-well plate. There is not a linear increase for the development of wavelength and amplitude but a steeper increase (after the 8th position) toward the end of the gradient. However, for the wrinkle, wavelength and amplitude are always coupled. In order to determine the optimum parameter promoting the osteogenic differentiation of hBM-MSCs, it is important to decouple these two parameters.

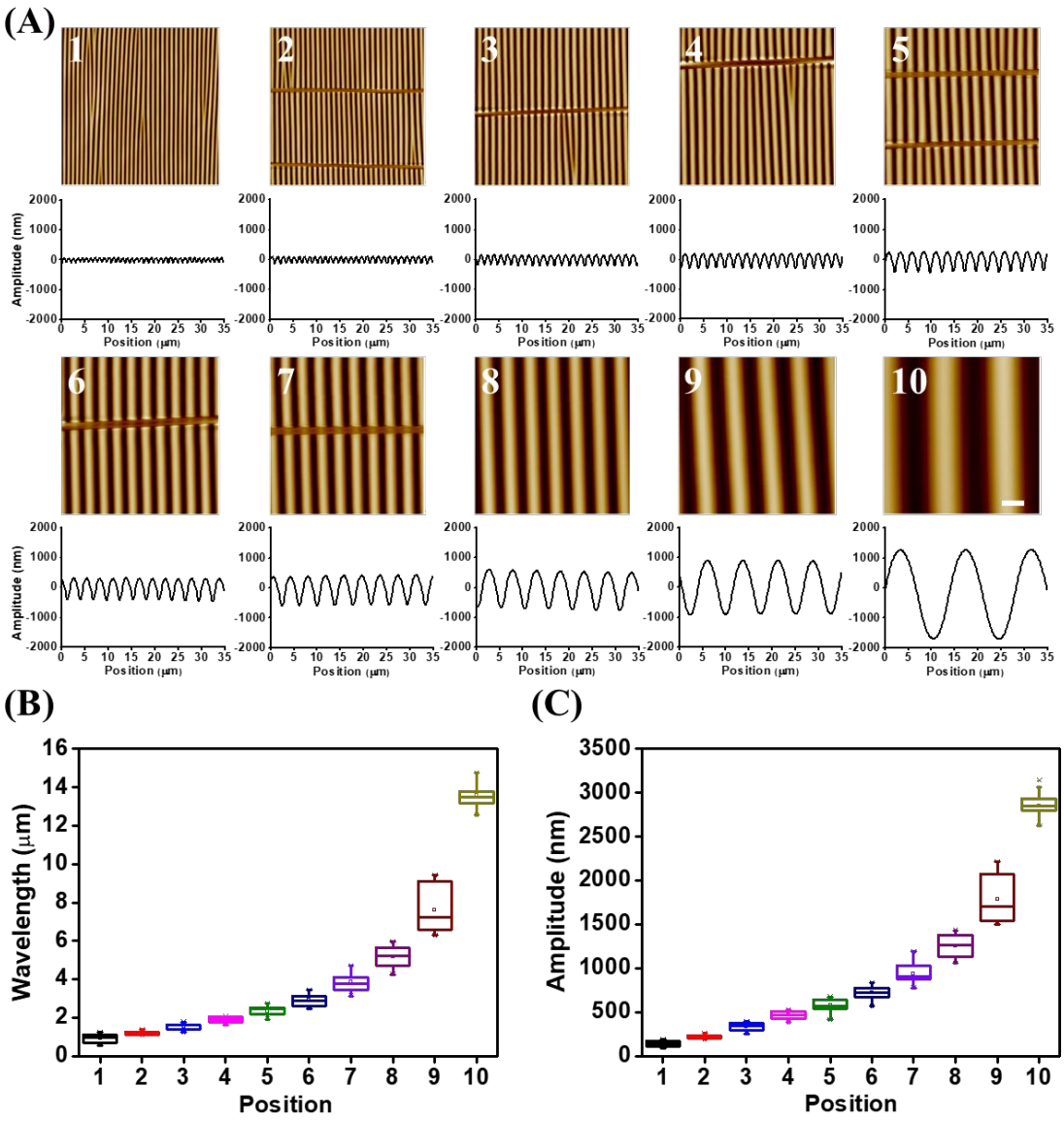

Figure 2. (A) Representative AFM images and amplitude curves of wrinkles along the gradient after imprinting. The number (1, 2, …10) in the AFM image stands for the column number in 96-well plate. Quantification analysis of wavelength (B) and amplitude (C) of the created wrinkle gradient. ≥30 wrinkles for each sample and three independent imprints were analyzed. Scale bar represents 5 μm.

4.3.2 Decoupling the amplitude via plasma oxidation

The surface of the substrate formed a bioglass-like (SiO_2) layer after the oxidation process[30]. Therefore, it is crucial for the mold to be imprinted into pristine PDMS before the second time plasma oxidation. The amplitude of the wrinkles were found to decrease when applying the second time plasma oxidation and longer time generated the lower amplitude (**Figure 3**). The oxidation provides stiffening and surface cross-linking. The combination of surface cross-linking, loss of the organic segments of the PDMS due to over-oxidation, and the transformation from an elastomeric to more organized phase most likely induces tension on the surface. As a result of this tension, the wrinkles are affected and it was found that particularly the amplitude was influenced the most resulting in reduction of the amplitude while the wavelength was found to remain the same. Therefore, in this way, the wavelength and amplitude were decoupled and control over the amount of amplitude reduction was achieved by altering the oxidation time. By shielding the rows sequentially, the high throughput platform was prepared by moving the mask gradually (**Figure 1A**).

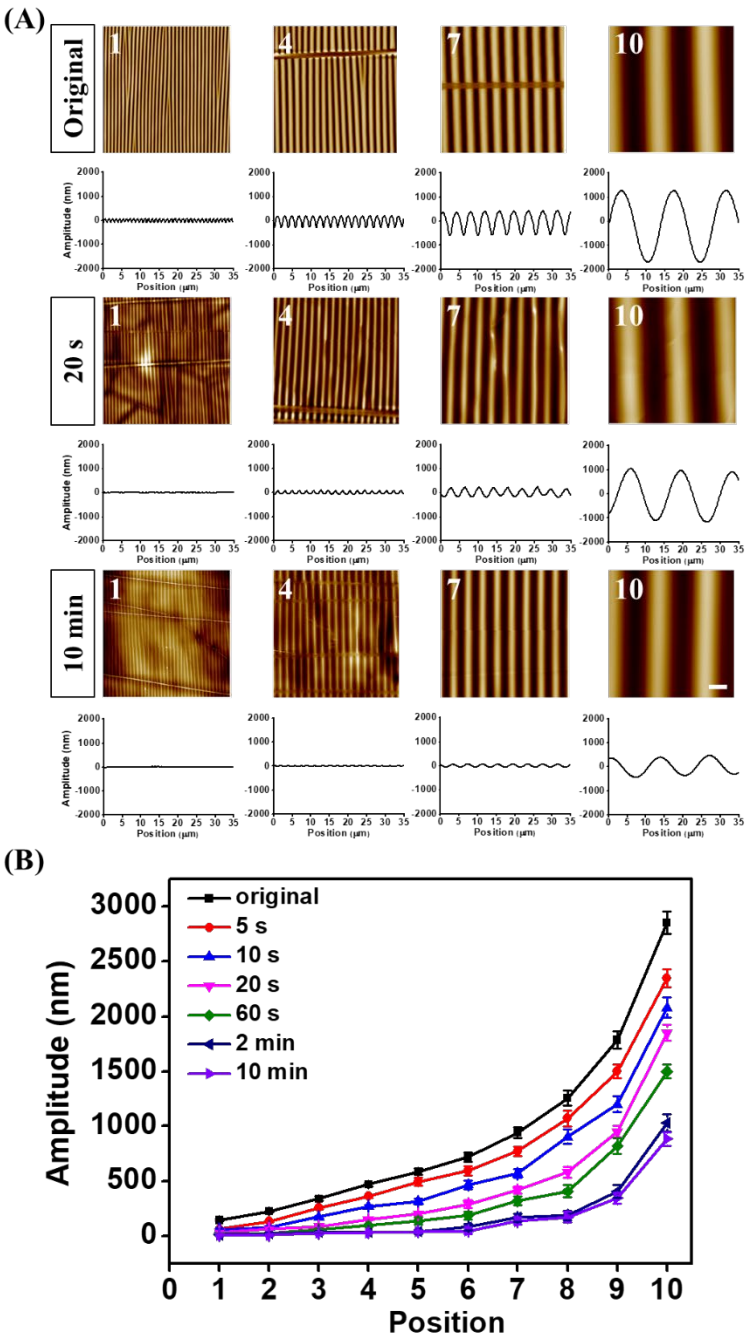

Figure 3. (A) Representative AFM images taken after imprinting and amplitude curves of the wrinkles along the gradient after different time (0 s, 20 s, 10 min) of plasma oxidation. (B) The variation curve of amplitude after the second time plasma oxidation. ≥30 wrinkles for each sample and three independent substrates were analyzed. Scale bar represents 5 μm.

As shown in **Figure 3**, after the plasma oxidation for different times, the wrinkle retained their shape but as observed from the height profiles, the amplitude decreased after the oxidation. Furthermore, a longer oxidation time resulted in a lower amplitude (**Figure 3A**). For column 1, the amplitude decreased from 144 nm to 6 nm while column 10 displayed a reduction in amplitude from 2854 nm to 833 nm (**Figure 3B**). Every row had the same wavelength development, while the wavelength was fixed within a column. However, within a column the amplitudes gradually decreased from row A to G. This approach provides the foundation for the HTS platform consisting of 70 different combinations of wavelengths and amplitudes. The substrate with 9.6 cm length and 7.5 cm width was chosen (**Figure S1**) to cover the area from column 1 to the middle of column 11. A flat control was placed in column 12. The integration of the substrates into a 96-well plate ensures proper handling since no variations in surface location are possible, a gradient

is highly susceptible to small differences in location. An additional important aspect is that it allows the technology to be used more broadly as the well plate technology is compatible with standardized equipment and able to be used by all without prior specific training.

4.3.3 Macroscopic behavior of hBM-MSCs modulated by wrinkle wavelength and amplitude

Cell elongation and orientation are crucial features for many anisotropic tissue functions[42]. Using the screening platform composed of different wavelengths and amplitudes as culture substrates, we investigated the influence on the morphology and orientation of hBM-MSCs. For this purpose, cells were cultured for 1 day on the substrates. As shown in **Figure 4A** (the image for all the wells are displayed in **Figure S2**), cell behavior was analyzed by TissueFaxs. From the fluorescence imaging of cells within the various wells, it is clearly shown that the cells became more oriented and elongated with increasing wavelength. For instance, compared to position G1, cells cultured on position G10 showed high elongation and orientation along the long axis of the wrinkles. There were similar trends for other rows. More importantly, for the same wavelength, with the decrease of amplitude, the morphology of cells changed from elongated and oriented to a more random shape (for example, A1 to G1).

Furthermore, cell area, cell elongation, and nucleus area were determined by TissueQuest. A 2D heat map representation originating from analysis of every well within the well-plate, showed the cell area, cell elongation and nucleus area after 24 h culture (**Figure 4B**, **4C**, and **Figure S3**). The cell spreading was visualized by analyzing phalloidin stained fiber actin. As shown in **Figure 4B,** the cell area is greatly influenced by the amplitude of wrinkle. The cell area increased with decreasing amplitude, which was observed in column 9 where the average cell area of 3651 μm² at the low amplitude side decreased to 1062 μm² at the higher amplitude side. This decrease was observed for all wavelengths and indicates that lower amplitude of wrinkle enhances the cell spreading and higher amplitude suppresses it.

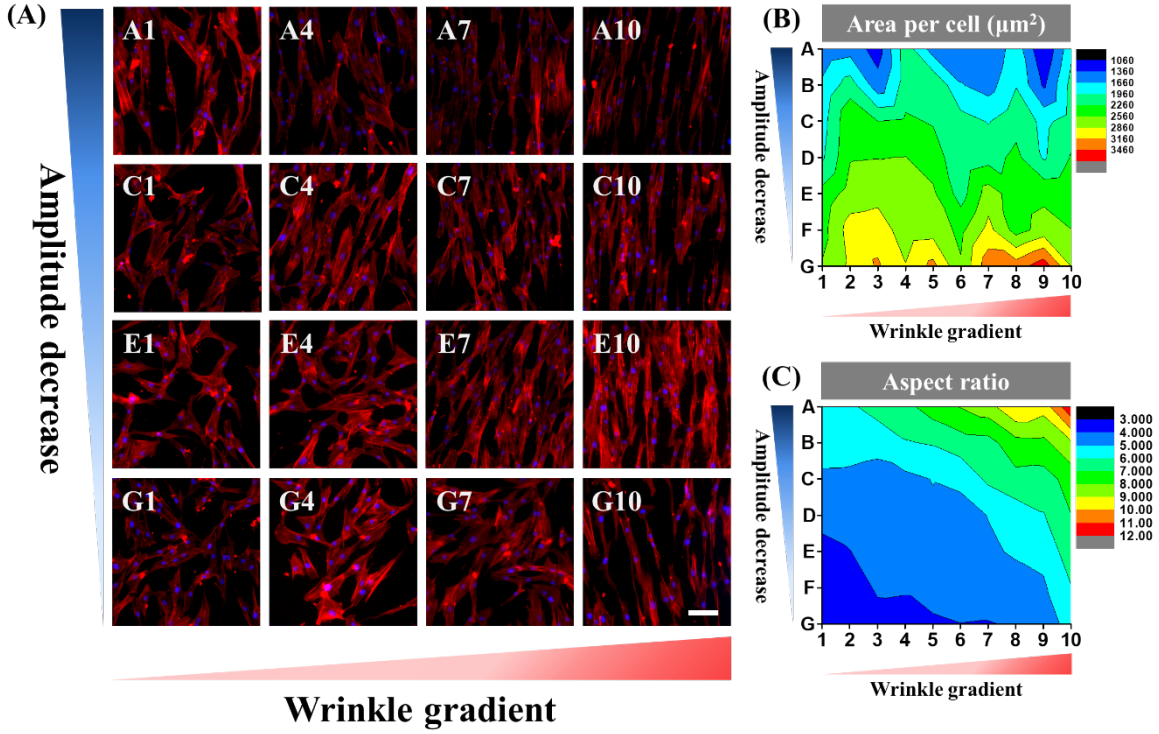

Figure 4. (A) Representative fluorescent images of hBM-MSCs cultured on different wells in the 96-well plate. TRITC-phalloidin (red) and DAPI (blue) was used to stain F-actin and cell nucleus, respectively. Scale bar represents 100 μm. 2D heat map representations of cell area (B) and cell aspect ratio (C) for the HTS platform (≥ 60 cells were analyzed). Each experiment was performed in triplicate.

The cell aspect ratio (C_{AR}) is an essential characterization of cell shape[43]. Moreover, the differentiation behavior of stem cells could be dramatically affected by AR[43–45]. As shown in **Figure 4C**, AR was adjusted synergistically by wavelength and amplitude. With the decreasing of amplitude, there has been a steep drop in the C_{AR}, suggesting that a higher amplitude enhances the C_{AR} and lower amplitudes suppresses it.

Furthermore, the C_{AR} increased with increasing wavelength, and the largest C_{AR} was found on the position A10 (AR: 11.83) which was the position with highest wavelength and amplitude. Several studies reported that different values for the C_{AR} have a great effect on the osteogenic and adipogenic differentiation of MSCs. Kilian and co-workers[45] examined three cases of C_{AR} (1, 1.5, 4), and found that adipogenesis decreased with C_{AR} and observed a monotonic increase of osteogenesis with increasing C_{AR}. Ding et al.[44] studied 6 cases of AR (1, 1.5, 2, 4, 8, 16), and found the same conclusion for adipogenic differentiation and 2 is the optimal for osteogenesis. Moreover, Ding et al.[43] revealed that C_{AR} itself is an inherent factor for guiding lineage commitment of MSCs, regardless of chemical factors. Although, these studies have provided valuable information, it is important to note that most studies focused on the C_{AR} with discrete values, not in a continuous way. In contrast, in this study, cells showed varied C_{AR} ranging from 3.42 to 11.83, which is advantageous to explore the influence of different C_{AR} on the fate commitment of stem cells.
The nucleus size is closely associated with nuclear function and cell differentiation[46]. It was found that cells exhibited larger nucleus area on the HTS platform with smaller amplitude (**Figure S3**). Cells grown on the small wrinkle side showed an increase in the nucleus area per cell with decreasing amplitude going from average nucleus area of 234 μm^2 at the low amplitude side to 139 μm^2 at the high amplitude side. Similarly, cells showed the same trend when cells were on the larger wrinkle side. Taken together, these results indicate that the amplitude of wrinkle has a significant influence on the cell spreading and morphology. Moreover, amplitude and wavelength have a combined role for these phenomena.

4.3.4 The optimum parameter of wrinkle for the osteogenesis of hBM-MSCs

To identify the optimum wrinkle parameter for osteogenic differentiation, hBM-MSCs were cultured in OM for 14 and 21 days. The osteogenic differentiation was evaluated by the immunofluorescent staining of ALP and Alizarin Red staining.

4.3.4.1 ALP expression

ALP activity is a marker for the osteogenesis of stem cells[47], and used to evaluate osteogenic differentiation of hBM-MSC[48]. For visualize the differentiation on the HTS platform, the cells were stained with the antibody against ALP after 2 weeks of culture. **Figure 5A** shows that hBM-MSCs displayed varied fluorescence density of ALP on the HTS platform. With the decrease of amplitude, a gradual rise in the intensity of ALP was observed followed by a drop, suggesting that the expression of ALP is significantly influenced by the amplitude of wrinkle. For the wrinkle gradient (X-axis), ALP expression displayed a similar trend as mentioned above. The expression was quantified by evaluating the intensity of fluorescence (**Figure 5B)**. The fluorescent intensity is normalized to the cell number and it indicates a good agreement with the qualitative analysis. The optimum positions on the HTS topography well plate for osteogenic differentiation were B4 and C3, and the corresponding parameters of wrinkles were W: 1.91 μm/A: 360 nm for B4, and 1.55 μm/173 nm for C3. Furthermore, ALP staining for representative positions (i.e., flat, B4, C3, D6, and F9) were displayed in **Figure 5C**.

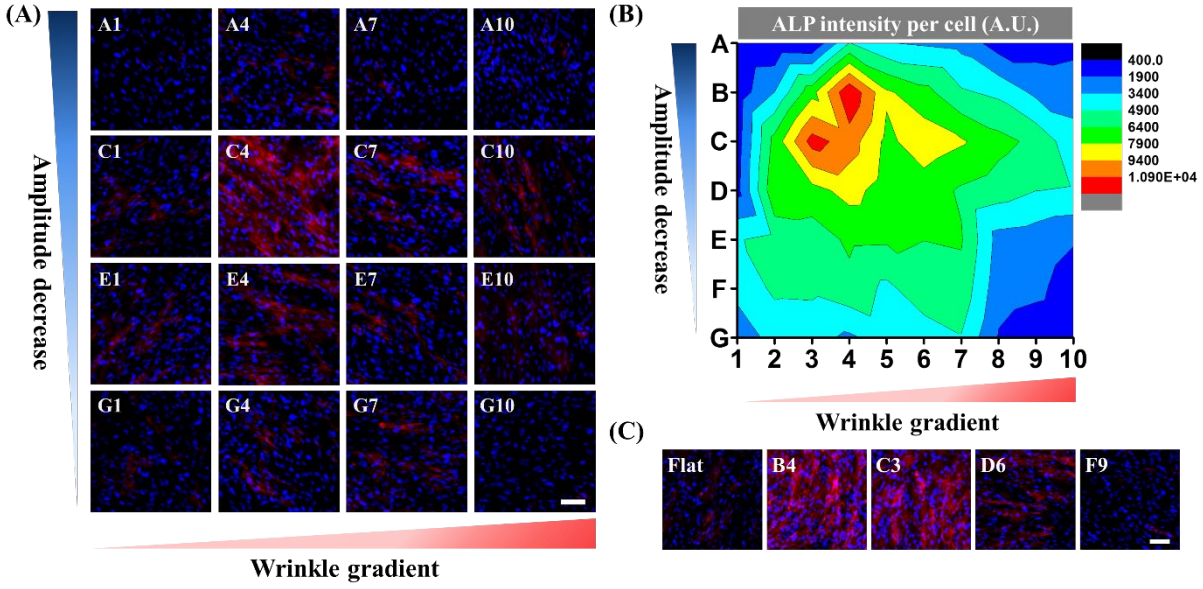

Figure 5. (A) Immunofluorescent staining of ALP for hBM-MSCs grown on the HTS platform cultured in OM for 14 days. Nucleus (blue) and ALP (red) were stained. (B) 2D heat map representations of the ALP intensity which was normalized by cell number (at least 50 cells were analyzed), and each experiment was performed in triplicate. (C) Immunofluorescent staining of ALP for hBM-MSCs grown on flat, B4, C3, D6, F9, cultured in OM for 14 days. Nucleus (blue) and ALP (red) were stained. Scale bar represents 100 μm.

4.3.4.2 Alizarin Red staining

Mineralization is an important indicator of osteoblasts, and the nodules can be stained by Alizarin Red, which is commonly used to evaluate the osteogenesis of stem cells[49]. From the results of ALP staining, the position B4, C3, D6, F9 (corresponded to the 96-well plate) and flat were selected, and the uniform substrates (suitable for 24-well plate) corresponding to the features of each of these positions were prepared for further study. Larger uniform substrates were prepared as the liquid handling (repetitive washing) within the 96-well plate was found to disturb the Alizarin Red stained nodules resulting in a less accurate read-out. For immunofluorescent staining this aspect was not a problem.

After 21 days in OM, the mineralized nodules on the substrates were stained by Alizarin Red (**Figure 6A**). hBM-MSCs grown on the substrate B4 showed the highest expression of mineralization compared to those on the substrate C3 and D6, while the expression on F9 and flat was rather minimal. The value of OD at 540nm was measured to further quantify the mineralization of hBM-MSC. As shown in **Figure 6B**, the highest OD_{540} was obtained for cells cultured on B4 followed by those on C3, which suggests the best osteogenic differentiation. The value was significantly lower for 9F and flat. The mineralization results are in consistent with the ALP expression. Taken together, these results indicate that the optimum parameter for osteogenic differentiation of stem cells is B4 (W: 1.91 μm/A: 360 nm) and that the 96-well plate with double topography parameter alterations is a valuable tool to identify topography-mediated cell responses.

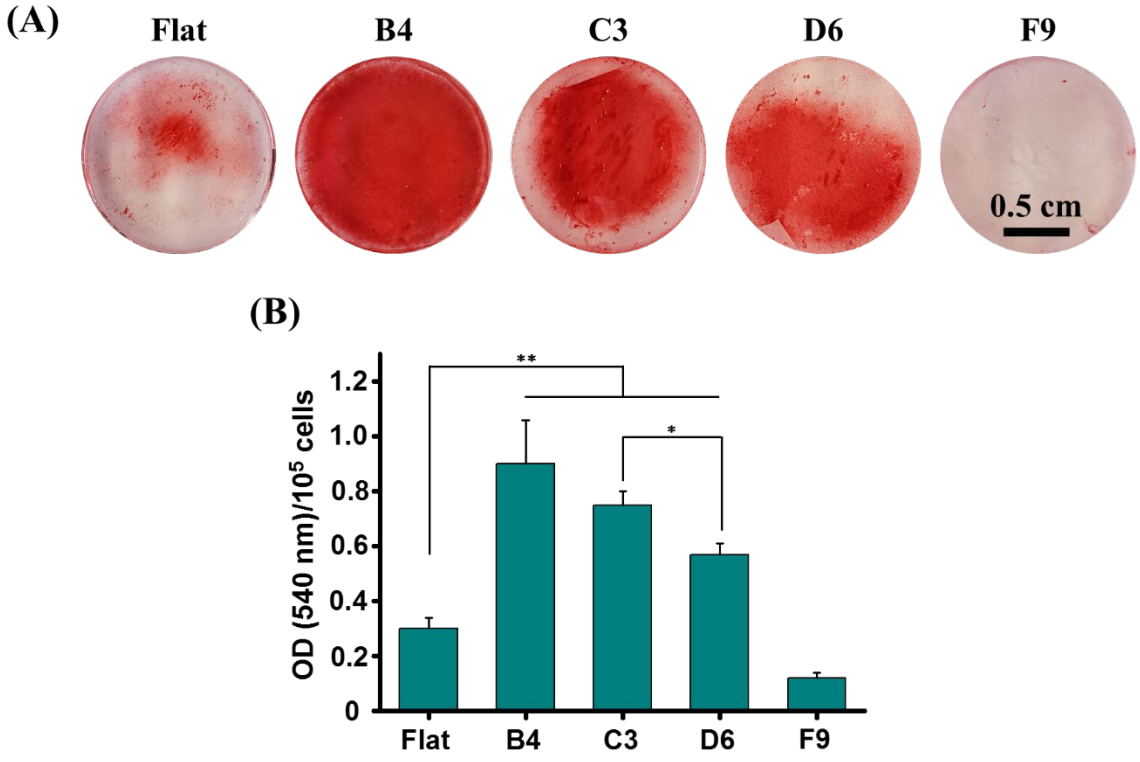

Figure 6. (A) Representative images of calcium stained with Alizarin Red for hBM-MSCs cultured in OM for 21 days. (B) Quantification of the extent of mineralization, normalized by cell number, and each experiment was performed in triplicate. Data are shown as mean ± standard deviation (SD), and $^{**}P < 0.01$, $^{*}P < 0.05$. Scale bar represents 0.5 cm.

4.4 Conclusion

The HTS platform consisting of 70 different combinations of wavelengths and amplitudes in one 96-well

plate was successfully prepared. The key feature is the possibility to decouple the wavelength and amplitude and thereby allowing to identify the contribution to cell behavior of both parameters. The results of the cell culture *in vitro* show that the cell area, elongation, and nucleus area were significantly influenced by the varied wrinkle parameters. Furthermore, hBM-MSCs showed different osteogenic differentiation capacity on the platform, and the optimum parameter for the wrinkle features was identified to be W: 1.91 µm/A: 360 nm (B4). The platform with a broad topography spectrum is an elegant substrate for the investigation of topography directing fate commitment of stem cells. Also, this versatile platform employed herein that is usable by all with standard approaches and equipment provides a powerful strategy for improving the development of biomaterials for bone tissue engineering.

4.5 References

(1) Vega, S. L.; Arvind, V.; Mishra, P.; Kohn, J.; Sanjeeva Murthy, N.; Moghe, P. V. Substrate Micropatterns Produced by Polymer Demixing Regulate Focal Adhesions, Actin Anisotropy, and Lineage Differentiation of Stem Cells. *Acta Biomater.* **2018**, *76*, 21–28.

(2) Pittenger, M. F. Multilineage Potential of Adult Human Mesenchymal Stem Cells. *Science.* **1999**, *284* (5411), 143–147.

(3) Zhang, L.; Ren, G.; Shi, Y.; Xu, G.; Yuan, Z.; Zhang, Y.; Zhao, R. C. Immunosuppressive Properties of Cloned Bone Marrow Mesenchymal Stem Cells IL-17 Signaling View Project IL-17C and Colon Cancer View Project Immunosuppressive Properties of Cloned Bone Marrow Mesenchymal Stem Cells. *Cell Res.* **2007**, *17*, 240–248.

(4) Caplan, A. I. Adult Mesenchymal Stem Cells for Tissue Engineering versus Regenerative Medicine. *Journal of Cellular Physiology.* **2007**, *213* (2), 341–347.

(5) Yang, J.; McNamara, L. E.; Gadegaard, N.; Alakpa, E. V.; Burgess, K. V.; Meek, R. M. D.; Dalby, M. J. Nanotopographical Induction of Osteogenesis through Adhesion, Bone Morphogenic Protein Cosignaling, and Regulation of MicroRNAs. *ACS Nano* **2014**, *8* (10), 9941–9953.

(6) Teo, B. K. K.; Wong, S. T.; Lim, C. K.; Kung, T. Y. S.; Yap, C. H.; Ramagopal, Y.; Romer, L. H.; Yim, E. K. F. Nanotopography Modulates Mechanotransduction of Stem Cells and Induces Differentiation through Focal Adhesion Kinase. *ACS Nano* **2013**, *7* (6), 4785–4798.

(7) Zhang, S.; Ma, B.; Liu, F.; Duan, J.; Wang, S.; Qiu, J.; Li, D.; Sang, Y.; Liu, C.; Liu, D.; Liu, H. Polylactic Acid Nanopillar Array-Driven Osteogenic Differentiation of Human Adipose-Derived Stem Cells Determined by Pillar Diameter. *Nano Lett.* **2018**, *18* (4), 2243–2253.

(8) Li, L.; Yang, S.; Xu, L.; Li, Y.; Fu, Y.; Zhang, H.; Song, J. Nanotopography on Titanium Promotes Osteogenesis via Autophagy-Mediated Signaling between YAP and β-Catenin. *Acta Biomater.* **2019**, *96*, 674–685.

(9) Stanton, A. E.; Tong, X.; Yang, F. Extracellular Matrix Type Modulates Mechanotransduction of Stem Cells. *Acta Biomater.* **2019**, *96*, 310–320.

(10) Dalby, M. J.; Gadegaard, N.; Oreffo, R. O. C. Harnessing Nanotopography and Integrin-Matrix Interactions to Influence Stem Cell Fate. *Nat. Mater.* **2014**, *13* (6), 558–569.

(11) Schaap-Oziemlak, A. M.; Kühn, P. T.; Van Kooten, T. G.; Van Rijn, P. Biomaterial-Stem Cell Interactions and Their Impact on Stem Cell Response. *RSC Adv.* **2014**, *4* (95), 53307–53320.

(12) Kim, J.; Kim, H. N.; Lim, K. T.; Kim, Y.; Pandey, S.; Garg, P.; Choung, Y. H.; Choung, P. H.; Suh, K. Y.; Chung, J. H. Synergistic Effects of Nanotopography and Co-Culture with Endothelial Cells on Osteogenesis of Mesenchymal Stem Cells. *Biomaterials* **2013**, *34* (30), 7257–7268.

(13) Dalby, M. J.; Riehle, M. O.; Johnstone, H.; Affrossman, S.; Curtis, A. S. G. Investigating the Limits of Filopodial Sensing: A Brief Report Using SEM to Image the Interaction between 10 Nm High Nano - topography and Fibroblast Filopodia. *Cell Biol. Int.* **2004**, *28* (3), 229–236.

(14) Dunn, G. A.; Heath, J. P. A New Hypothesis of Contact Guidance in Tissue Cells. *Exp. Cell Res.* **1976**, *101* (1), 1–14.

(15) Seo, C. H.; Jeong, H.; Feng, Y.; Montagne, K.; Ushida, T.; Suzuki, Y.; Furukawa, K. S. Micropit Surfaces Designed for Accelerating Osteogenic Differentiation of Murine Mesenchymal Stem Cells via Enhancing Focal Adhesion and Actin Polymerization. *Biomaterials* **2014**, *35* (7), 2245–2252.

(16) Seo, C. H.; Furukawa, K.; Montagne, K.; Jeong, H.; Ushida, T. The Effect of Substrate Microtopography on Focal Adhesion Maturation and Actin Organization via the RhoA/ROCK Pathway. *Biomaterials* **2011**, *32* (36), 9568–9575.

(17) Wang, W.; Zhao, L.; Wu, K.; Ma, Q.; Mei, S.; Chu, P. K.; Wang, Q.; Zhang, Y. The Role of Integrin-Linked Kinase/β-Catenin Pathway in the Enhanced MG63 Differentiation by Micro/Nano-Textured Topography. *Biomaterials* **2013**, *34* (3), 631–640.

(18) Wang, W.; Liu, Q.; Zhang, Y.; Zhao, L. Involvement of ILK/ERK1/2 and ILK/P38 Pathways in Mediating the Enhanced Osteoblast Differentiation by Micro/Nanotopography. *Acta Biomater.* **2014**, *10* (8), 3705–3715.

(19) Niu, H.; Lin, D.; Tang, W.; Ma, Y.; Duan, B.; Yuan, Y.; Liu, C. Surface Topography Regulates Osteogenic Differentiation of MSCs via Crosstalk between FAK/MAPK and ILK/β-Catenin Pathways in a Hierarchically Porous Environment. *ACS Biomater. Sci. Eng.* **2017**, *3* (12), 3161–3175.

(20) Wegst, U. G. K.; Bai, H.; Saiz, E.; Tomsia, A. P.; Ritchie, R. O. Bioinspired Structural Materials. *Nat. Mater.* **2015**, *14* (1), 23–36.

(21) Yin, Z.; Chen, X.; Chen, J. L.; Shen, W. L.; Hieu Nguyen, T. M.; Gao, L.; Ouyang, H. W. The Regulation of Tendon Stem Cell Differentiation by the Alignment of Nanofibers. *Biomaterials* **2010**, *31* (8), 2163–2175.
(22) Engelmayr, G. C.; Cheng, M.; Bettinger, C. J.; Borenstein, J. T.; Langer, R.; Freed, L. E. Accordion-like Honeycombs for Tissue Engineering of Cardiac Anisotropy. *Nat. Mater.* **2008**, *7* (12), 1003–1010.
(23) Georgiou, M.; Bunting, S. C. J.; Davies, H. A.; Loughlin, A. J.; Golding, J. P.; Phillips, J. B. Engineered Neural Tissue for Peripheral Nerve Repair. *Biomaterials* **2013**, *34* (30), 7335–7343.
(24) Kukumberg, M.; Yao, J. Y.; Neo, D. J. H.; Yim, E. K. F. Microlens Topography Combined with Vascular Endothelial Growth Factor Induces Endothelial Differentiation of Human Mesenchymal Stem Cells into Vasculogenic Progenitors. *Biomaterials* **2017**, *131*, 68–85.
(25) Tan, K. K. B.; Tann, J. Y.; Sathe, S. R.; Goh, S. H.; Ma, D.; Goh, E. L. K.; Yim, E. K. F. Enhanced Differentiation of Neural Progenitor Cells into Neurons of the Mesencephalic Dopaminergic Subtype on Topographical Patterns. *Biomaterials* **2015**, *43* (1), 32–43.
(26) Faia-Torres, A. B.; Guimond-Lischer, S.; Rottmar, M.; Charnley, M.; Goren, T.; Maniura-Weber, K.; Spencer, N. D.; Reis, R. L.; Textor, M.; Neves, N. M. Differential Regulation of Osteogenic Differentiation of Stem Cells on Surface Roughness Gradients. *Biomaterials* **2014**, *35* (33), 9023–9032.
(27) Kim, D. H.; Han, K.; Gupta, K.; Kwon, K. W.; Suh, K. Y.; Levchenko, A. Mechanosensitivity of Fibroblast Cell Shape and Movement to Anisotropic Substratum Topography Gradients. *Biomaterials* **2009**, *30* (29), 5433–5444.
(28) Kim, D. H.; Seo, C. H.; Han, K.; Kwon, K. W.; Levchenko, A.; Suh, K. Y. Guided Cell Migration on Microtextured Substrates with Variable Local Density and Anisotropy. *Adv. Funct. Mater.* **2009**, *19* (10), 1579–1586.
(29) Beijer, N. R. M.; Vasilevich, A. S.; Pilavci, B.; Truckenmüller, R. K.; Zhao, Y.; Singh, S.; Papenburg, B. J.; de Boer, J. TopoWellPlate: A Well-Plate-Based Screening Platform to Study Cell-Surface Topography Interactions. *Adv. Biosyst.* **2017**, *1* (4), 1700002.
(30) Zhou, Q.; Castañeda Ocampo, O.; Guimarães, C. F.; Kühn, P. T.; Van Kooten, T. G.; Van Rijn, P. Screening Platform for Cell Contact Guidance Based on Inorganic Biomaterial Micro/Nanotopographical Gradients. *ACS Appl. Mater. Interfaces* **2017**, *9* (37), 31433–31445.
(31) Liguori, G. R.; Zhou, Q.; Liguori, T. T. A.; Barros, G. G.; Kühn, P. T.; Moreira, L. F. P.; van Rijn, P.; Harmsen, M. C. Directional Topography Influences Adipose Mesenchymal Stromal Cell Plasticity: Prospects for Tissue Engineering and Fibrosis. *Stem Cells Int.* **2019**, *2019*, 5387850.
(32) Almonacid Suarez, A. M.; Zhou, Q.; Van Rijn, P.; Harmsen, M. C. Directional Topography Gradients Drive Optimum Alignment and Differentiation of Human Satellite Cells. *J Tissue Eng Regen Med.* **2019**, *13* (12), 2234–2245.
(33) Abagnale, G.; Sechi, A.; Steger, M.; Zhou, Q.; Kuo, C. C.; Aydin, G.; Schalla, C.; Müller-Newen, G.; Zenke, M.; Costa, I. G.; van Rijn, P.; Gillner, A.; Wagner, W. Surface Topography Guides Morphology and Spatial Patterning of Induced Pluripotent Stem Cell Colonies. *Stem Cell Reports* **2017**, *9* (2), 654–666.
(34) Ge, L.; Yang, L.; Bron, R.; Burgess, J. K.; Van Rijn, P. Topography-Mediated Fibroblast Cell Migration Is Influenced by Direction, Wavelength, and Amplitude. *ACS Appl. Bio Mater.* **2020**, *3* (4), 2104–2116.
(35) Yang, L.; Gao, Q.; Ge, L.; Zhou, Q.; M. Warszawik, E.; Bron, R.; Wai Chiu Lai, K.; Van Rijn, P. Topography Induced Stiffness Alteration of Stem Cells Influences Osteogenic Differentiation. *Biomater. Sci.* **2020**, in press, DOI: 10.1039/d0bm00264j.
(36) Yang, L.; Ge, L.; Zhou, Q.; Mokabber, T.; Pei, Y.; Bron, R.; Van Rijn, P. Biomimetic Multiscale Hierarchical Topography Enhances Osteogenic Differentiation of Human Mesenchymal Stem Cells. *Adv. Mater. Interfaces* **2020**, in press, DOI: 10.1002/admi.202000385.
(37) Yang, L.; Malgorzata Jurczak, K.; Ge, L.; Van Rijn, P. High Throughput Screening and Hierarchical Topography-Mediated Neural Differentiation of Mesenchymal Stem Cells. *Adv. Healthc. Mater.* **2020**, in press, DOI: 10.1002/adhm.202000117.
(38) Choi, Y.-J.; Park, S. J.; Yi, H.-G.; Lee, H.; Kim, D. S.; Cho, D.-W. Muscle-Derived Extracellular Matrix on Sinusoidal Wavy Surfaces Synergistically Promotes Myogenic Differentiation and Maturation. *J. Mater. Chem. B* **2018**, *6* (35), 5530–5539.
(39) Song, K. H.; Park, S. J.; Kim, D. S.; Doh, J. Sinusoidal Wavy Surfaces for Curvature-Guided Migration of Tlymphocytes. *Biomaterials* **2015**, *51*, 151–160.

(40) van der Boon, T. A. B.; Yang, L.; Li, L.; Córdova Galván, D. E.; Zhou, Q.; de Boer, J.; van Rijn, P. Well Plate Integrated Topography Gradient Screening Technology for Studying Cell-Surface Topography Interactions. *Adv. Biosyst.* **2019**, *1900218*.
(41) Lee, J. S.; Hong, H.; Park, S. J.; Lee, S. J.; Kim, D. S. A Simple Fabrication Process for Stepwise Gradient Wrinkle Pattern with Spatially-Controlled Wavelength Based on Sequential Oxygen Plasma Treatment. *Microelectron. Eng.* **2017**, *176*, 101–105.
(42) Prager-Khoutorsky, M.; Lichtenstein, A.; Krishnan, R.; Rajendran, K.; Mayo, A.; Kam, Z.; Geiger, B.; Bershadsky, A. D. Fibroblast Polarization Is a Matrix-Rigidity-Dependent Process Controlled by Focal Adhesion Mechanosensing. *Nat. Cell Biol.* **2011**, *13* (12), 1457–1465.
(43) Yao, X.; Peng, R.; Ding, J. Effects of Aspect Ratios of Stem Cells on Lineage Commitments with and without Induction Media. *Biomaterials* **2013**, *34* (4), 930–939.
(44) Peng, R.; Yao, X.; Ding, J. Effect of Cell Anisotropy on Differentiation of Stem Cells on Micropatterned Surfaces through the Controlled Single Cell Adhesion. *Biomaterials* **2011**, *32* (32), 8048–8057.
(45) Kilian, K. A.; Bugarija, B.; Lahn, B. T.; Mrksich, M. Geometric Cues for Directing the Differentiation of Mesenchymal Stem Cells. *Proc. Natl. Acad. Sci.* **2010**, *107* (11), 4872–4877.
(46) Liu, X.; Liu, R.; Cao, B.; Ye, K.; Li, S.; Gu, Y.; Pan, Z.; Ding, J. Subcellular Cell Geometry on Micropillars Regulates Stem Cell Differentiation. *Biomaterials* **2016**, *111*, 27–39.
(47) Kim, I. G.; Hwang, M. P.; Du, P.; Ko, J.; Ha, C. won; Do, S. H.; Park, K. Bioactive Cell-Derived Matrices Combined with Polymer Mesh Scaffold for Osteogenesis and Bone Healing. *Biomaterials* **2015**, *50* (1), 75–86.
(48) Li, J.; Mou, X.; Qiu, J.; Wang, S.; Wang, D.; Sun, D.; Guo, W.; Li, D.; Kumar, A.; Yang, X.; Li, A.; Liu, H. Surface Charge Regulation of Osteogenic Differentiation of Mesenchymal Stem Cell on Polarized Ferroelectric Crystal Substrate. *Adv. Healthc. Mater.* **2015**, *4* (7), 998–1003.
(49) Qiu, J.; Li, J.; Wang, S.; Ma, B.; Zhang, S.; Guo, W.; Zhang, X.; Tang, W.; Sang, Y.; Liu, H. TiO2 Nanorod Array Constructed Nanotopography for Regulation of Mesenchymal Stem Cells Fate and the Realization of Location-Committed Stem Cell Differentiation. *Small* **2016**, *12* (13), 1770–1778.